High-speed and high-resolution interrogation of FBG sensors using wavelength-to-time mapping and Gaussian filters

MANUEL P. FERNÁNDEZ,[1,2,5] **LAUREANO A. BULUS ROSSINI,**[1,2]
JOSÉ L. CRUZ,[3] **MIGUEL V. ANDRÉS,**[3] **AND PABLO A. COSTANZO
CASO**[1,2,4]

[1]*LIAT, Comisión Nacional de Energía Atómica (CNEA) & Instituto Balseiro (UNCuyo-CNEA), Bustillo 9500, Bariloche 8400 (RN), Argentina*
[2]*CONICET, CCT Patagonia Norte, Bariloche 8400 (RN), Argentina*
[3]*Departamento de Física Aplicada y Electromagnetismo, Universidad de Valencia, Moliner 50, Spain*
[4]*pcostanzo@ib.edu.ar*
[5]*manuel.fernandez@ib.edu.ar*

Abstract: In this work we report a novel intensity-based technique for simultaneous high-speed and high-resolution interrogation of fiber Bragg grating (FBG) sensors. The method uses a couple of intensity Gaussian filters and the dispersion-induced wavelength-to-time mapping effect. The Bragg wavelength is retrieved by means of the amplitude comparison between the two filtered grating spectrums, which are mapped into a time-domain waveform. In this way, measurement distortions arising from residual power due to the grating sidelobes are completely avoided, and the wavelength measurement range is considerably extended with respect to the previously proposed schemes. We present the mathematical background for the interrogation of FBGs with an arbitrary bandwidth. In our proof-of-concept experiments, we achieved sensitivities of ~20 pm with ultra-fast rates up to 264 MHz.

1. Introduction

Bragg gratings are among the most popular optical devices and they find applications in a wide variety of fields such as optical signal processing [1,2], optical communications and network monitoring [3–5], microwave photonics [6], and sensing [7,8]. In this sense, fiber Bragg grating (FBG) sensors are based on wavelength modulation, in which the sensed parameter (e.g. strain or temperature) is linearly related to the grating central wavelength [9].

The most extended FBG interrogation techniques use static filters to convert the wavelength shift into an intensity change. Among these methods, the edge filter [10,11], in which the detected light intensity is proportional to the wavelength drift, has attracted more attention due to its simple, low-cost and reliable structure. Interrogation of FBG sensors with speeds up to hundreds of megahertz is desirable in applications such as monitoring of ultra-fast dynamic phenomena, e.g. molecular dynamics sensing and in aerospace diagnostics. To this end, techniques based on the wavelength-to-time mapping using broadband pulses and dispersive components have been demonstrated [12–15]. These schemes have the shortcoming arising from the tradeoff between wavelength resolution and interrogation speed: high dispersions are required to achieve fine resolutions, leading to a limited maximum pulse repetition rate.

The conventional intensity-based methods require to be operated in the linear range of a filter to ensure a linear detection. Recently, Cheng et al. [16] proposed an interrogation system in which the linear dependence is achieved using Gaussian filters. The difference between the intensities at the output of two crossed Gaussian filters ultimately leads to a linear behavior, which is exploited for the Bragg wavelength determination. This scheme features the high sensitivity typical of

edge-filtering techniques and a flexibility in the selection of the sensitivity by simply adjusting the filters' offset. Moreover, it has been shown to be a promising solution for interrogation of FBGs with a wide spectrum [17]. However, the wavelength range in which the system shows a linear dependence is limited as power reflected from the grating sidelobes become non-negligible [17–18]. In fact, this shortcoming is common to every filtering-based techniques.

In this work, to solve this drawback, we propose and demonstrate a novel FBG interrogation technique based on crossed Gaussian filters, in which the filtered grating spectrum is mapped into a temporal waveform using a highly dispersive medium. The Bragg wavelength is then retrieved from the amplitude comparison between the time-mapped grating main lobes at the output of each filter. Consequently, measurement distortions arising from residual power due to the FBG side lobes are avoided, and the linear operational range is considerably extended. Moreover, in contrast to previous works in which the FBG spectral width must be either much narrower [16] or equal [17] to that of the Gaussian filters, we generalize the method for FBG sensors having an arbitrary spectral bandwidth, so the proposed system is further improved in terms of flexibility. Theoretical analysis and experimental results are presented and discussed.

2. Measurement principle

2.1. Mathematical background

Figure 1 illustrates the principle of the proposed FBG wavelength monitoring system. An optical source emits short broadband pulses at a repetition rate equal to the required interrogation speed. The pulses propagate through a highly dispersive medium with accumulated dispersion parameter D (in ps/nm). The resulting linearly-chirped pulse is used as probe pulse and transmitted to the sensing FBG, which is characterized by a reflectivity transfer function $R(\lambda)$. The reflected signal is then divided into two branches (branch 1 and 2) that present a couple of Gaussian filters with transfer functions $F_1(\lambda)$ and $F_2(\lambda)$. The signals at the output of the filters are detected and digitalized by separate photodiodes.
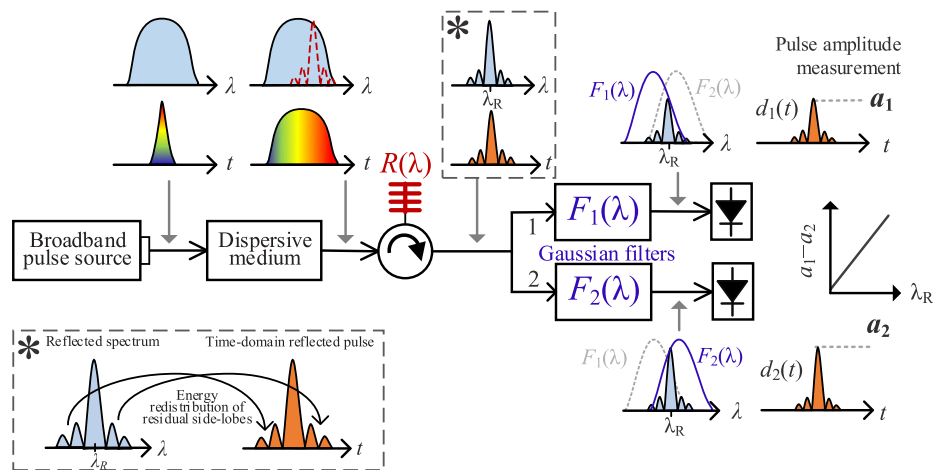

Fig. 1. Schematic representation of the FBG interrogation system based on the wavelength-to-time mapping and Gaussian filters. The inset of the figure (*) illustrates how the energy corresponding to the FBG side-lobes is re-arranged into temporal side-lobes in the time-domain waveform, as a result of the linear wavelength-to-time mapping.

If the dispersion D is large enough such that the far-field Fraunhofer condition is satisfied [19,20], the pulse spectrum is mapped into its temporal waveform with a wavelength-time relation given by the dispersion parameter. Assuming that the source spectrum is flat within the reflection

spectrum of the FBG, and that the FBG has negligible chirp compared to that of the highly dispersive medium, the detected signals at the output of branches 1 and 2 can be expressed as

$$d_i(t) \propto R(\lambda')F_i(\lambda') \quad i = 1, 2 \tag{1}$$

where $\lambda' = t / D$ is the wavelength-time scale [19–20]. Equation (1) implies that the overall system transfer function for each path, constituted by the product of the FBG and each Gaussian filter transfer functions, is mapped into the temporal waveform of the detected signals, with a time-wavelength scale determined by the accumulated dispersion D.

The Gaussian filters have both similar bandwidth B_F, and different central wavelength, λ_{F1} and λ_{F2}. On the other hand, the main lobe of the FBG can be accurately described by a Gaussian function with bandwidth B_R and central wavelength λ_R, especially for a low κL parameter [21,22]. Thus, we can write the FBG and the Gaussian filters transfer functions as

$$R(\lambda) \propto \exp\left(-4\ln(2)\left(\frac{\lambda - \lambda_R}{B_R}\right)^2\right), \quad \text{and} \quad F_i(\lambda) = \exp\left(-4\ln(2)\left(\frac{\lambda - \lambda_{Fi}}{B_F}\right)^2\right) \quad i = 1, 2. \tag{2}$$

By substituting Eqs. (2) into Eq. (1) we find that the detected waveform at the output of each branch $d_i(t)$ can be expressed as

$$d_i(t) = k \exp\left(-4\ln(2)\frac{(\lambda_R - \lambda_{Fi})^2}{B_R^2 + B_F^2}\right) \exp\left(-4\ln(2)\left(\frac{t - \tau_{di}}{T_d}\right)^2\right) \quad i = 1, 2, \tag{3}$$

where k is a constant that includes the power of the probe pulse and different coefficients that are identical in both paths, e.g. propagation losses and splitting losses. The pulse full-width at half-maximum T_d and its relative delay τ_{di} are given by

$$T_d = D\frac{B_R B_F}{\sqrt{B_R^2 + B_F^2}} \quad \tau_{di} = D\frac{\lambda_R B_F^2 + \lambda_{Fi} B_R^2}{B_F^2 + B_R^2}. \tag{4}$$

Let us define the amplitude of the detected pulses of Eq. (3) in dB units as $a_i = 10\log(\max\{d_i(t)\})$, $i = 1,2$. A linear dependence with the Bragg wavelength is achieved from the difference between the amplitudes of the detected signals in both channels. The amplitude comparison function (ACF) can be defined as the difference between both amplitudes, as follows

$$\text{ACF}(\lambda_R) = a_1 - a_2 = \frac{-40\log(e)\ln(2)(\lambda_{F1}^2 - \lambda_{F2}^2)}{B_R^2 + B_F^2} + \frac{80\log(e)\ln(2)(\lambda_{F1} - \lambda_{F2})}{B_R^2 + B_F^2}\lambda_R. \tag{5}$$

From Eq. (5) it can be noted that the ACF presents a linear dependence with the Bragg wavelength λ_R. The slope of the ACF, which determines the systems' sensitivity, can be tuned by adjusting the wavelength offset of the Gaussian filters, $\lambda_{F1} - \lambda_{F2}$, and it also depends on the filters and grating bandwidths, B_F and B_R.

Therefore, by means of a pulse-by-pulse digital signal processing, the grating Bragg wavelength can be retrieved from the measured pulses amplitude, $\tilde{a}_1$ and $\tilde{a}_2$, by applying the inverse amplitude comparison function $\lambda_R = \text{ACF}^{-1}(\tilde{a}_1 - \tilde{a}_2)$.

It is useful to compare the ACF of Eq. (5) with the difference between the Gaussian filters transfer functions (in dB). After some mathematical manipulations, it is straightforward to arrive to the following relation

$$\text{ACF}(\lambda_R) = \frac{B_F^2}{B_F^2 + B_R^2}(F_1(\lambda_R) - F_2(\lambda_R)). \tag{6}$$

Therefore, if the sensing FBG is much narrower than the Gaussian filters, such that $B_F{}^2 \gg B_R{}^2$, the amplitude comparison function is equal to the Gaussian filters difference. As the relative

grating bandwidth increases, the slope of the ACF decreases. For instance, in the limit $B_F = B_R$, it is reduced to one-half of its maximum.

2.2. Sidelobes consideration

Power arising from the FBG residual sidelobes are the main factor limiting the linear operational range in the conventional measurement method, which involves the differential detection of the overall output power P_i, i.e. the integral of the product $R(\lambda)F_i(\lambda)$ [17,18]. Nevertheless, in the proposed method, the grating sidelobes are temporally separated from the main lobe in the detected signal due to the wavelength-to-time mapping, and thus, they do not contribute to the amplitude measurement.

This feature allows to extend the linear measurement range, as exemplified in Fig. 2. For instance, Fig. 2(a) shows the Gaussian filters transfer functions where the wavelength offset is $\lambda_{F1} - \lambda_{F2} = 1.2$ nm and $B_F = 1.5$ nm, and a simulated spectrum of a uniform FBG with parameter $\kappa L = 0.6$, which yields a 3 dB bandwidth of $B_R = 415$ pm [21]. Figure 2(b) depicts the filtered FBG spectrum at the output of the two Gaussian filters. For instance, we illustrate the functions $R(\lambda)F_1(\lambda)$ (corresponding to Branch 1) and $R(\lambda)F_2(\lambda)$ (corresponding to Branch 2). Here, the spectrums are normalized in amplitude for illustration purposes. As it is seen, the FBG spectrum is approaching the edge of $F_1(\lambda)$ and, consequently, the energy of the residual sidelobes is comparable to that of the main lobe, therefore having non-negligible contribution to the output power, P_1. Figure 2(c) compares the maximum amplitude difference $a_1 - a_2$ and the overall power difference $P_1 - P_2$ as a function of the FBG central wavelength. Specifically, we show two cases in which $B_F = 1.5$ nm (solid lines) and $B_F = 1.75$ nm (dotted lines). The slope of the linear functions are found to be -11.93 dB/nm and -9.43 dB/nm, respectively, in accordance to that expected from Eq. (5). In both cases the linear range is extended using the amplitude comparison method (blue lines), for which the linear trend is only broken when the residual sidelobes amplitude at the output of the Gaussian filters are higher than the main lobe amplitude. Additionally, higher values of B_F lead to increased achievable linear range, as it is seen in the example of Fig. 2(c), where the linear range for $B_F = 1.75$ nm is 0.84 nm higher than that for $B_F = 1.5$ nm.
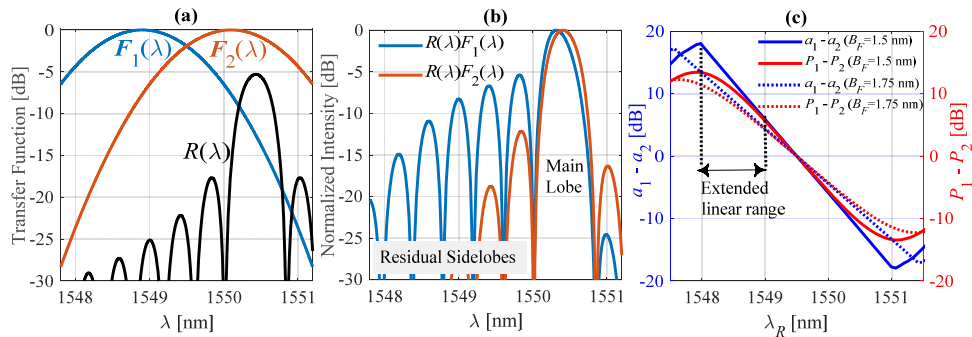

Fig. 2. (a) Transfer function of Gaussian filters and FBG reflectivity spectrum. (b) Filtered signal spectrum at the output of the two branches. (c) Comparison between the amplitude difference ($a_1 - a_2$) and the overall power difference ($P_1 - P_2$).

3. Experiments and discussion

In order to probe the measurement principle and evaluate its performance, we implemented the experimental setup illustrated in Fig. 3. As optical source, we used a pulsed laser (Onefive Origami 15) that emits high peak-power picosecond pulses centered at 1550 nm at a tunable

repetition rate. The pulses first propagate through a non-zero dispersion-shifted fiber spool in order to broaden their spectrum so it is approximately flat within the working wavelength range. Then, the pulses are attenuated and they propagate in the linear regime through the highly dispersive medium, which is a dispersion compensation module (DCM) with dispersion parameter $D = -1665.7$ ps/nm. The resulting linearly chirped pulses are amplified and a band-pass filter (BPF) with flat response is used to improve the noise isolation of the overall system. The pulse is then launched to the sensing FBG through an optical circulator. A 3 dB coupler derives the reflected signal to a couple of tunable optical filters (TOF) with Gaussian transmittance and approximately equal bandwidths of $B_F = 1.4$ nm. The output signals are detected using similar photodiodes (Thorlabs DET08CFC) with a bandwidth of 5 GHz and digitized using a real-time oscilloscope (Rhode & Schwarz RTO 1044) with a bandwidth of 4 GHz.
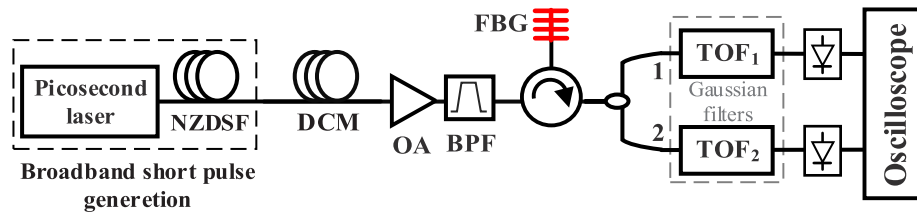

Fig. 3. Experimental setup of the FBG interrogation system. NZDSF: Non-zero Dispersion-shifted Fiber, DCM: Dispersion Compensation Module, OA: Optical Amplifier, BFP: Band-pass Filter, TOF: Tunable Optical Filter.

Firstly, we experimentally compared the achievable measurement range when a FBG is interrogated using the proposed method (based on the amplitude comparison $a_1 - a_2$) to that using the conventional method (based of the overall power difference $P_1 - P_2$). In our setup, the overall powers P_i are obtained by substituting the photodetectors at the branches' output by two power meters. We obtained both the maximum amplitude difference and the power difference at the output of each branch as a function of the FBG central wavelength, whose results are shown in Fig. 4(a). In this case, the Gaussian filters are set to have wavelength offsets of 1.04 nm and 1.46 nm around a central wavelength of 1549.5 nm. The first thing to note in Fig. 4(a) is that the sensitivity, i.e. the slope of the function, is higher as the filter offset increases, as expected from Eq. (5). Moreover, it is seen that the linear trend is significantly extended when using the amplitude comparison method, since residual power reflected from the FBG sidelobes is avoided as it was expected from the numerical simulations (see Fig. 2(c)).
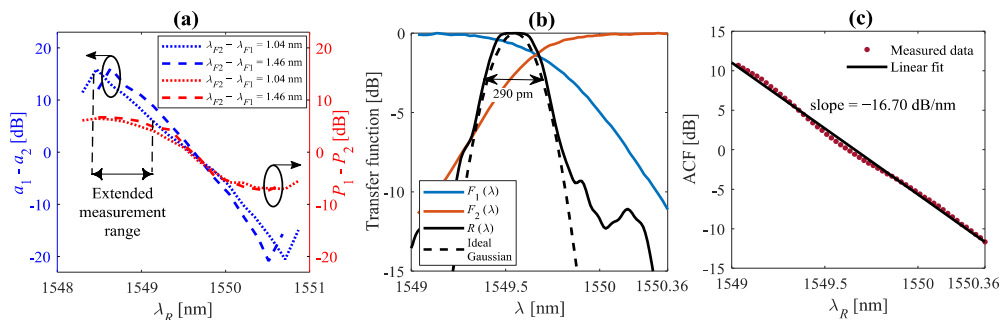

Fig. 4. (a) Linear wavelength range comparison for different filter offsets. (b) Measured Gaussian filters and FBG reflectivity spectrum. (c) Measured amplitude comparison function and linear fit.

In the following tests we fixed the filters' central wavelengths to $\lambda_{F1} = 1549$ nm (branch 1) and $\lambda_{F2} = 1550.3$ nm (branch 2). Therefore, the filters' wavelength offset is 1.3 nm. Figure 4(b) depicts the measured Gaussian filters transfer functions and the normalized reflectivity of the sensing FBG used in the experiments. The FBG main lobe is well adjusted by a Gaussian function with bandwidth $B_R = 0.29$ nm. The ACF for this setup is depicted in Fig. 4(c), which has been obtained from Eq. (6) by multiplying the measured filters difference data, $F_1 - F_2$, by the factor $B_F^2/(B_F^2 + B_R^2) = 0.96$. Together with the measured data it is plotted the corresponding linear fit, which presents a slope of -16.70 dB/nm.

The wavelength-to-time mapping of the filtered FBG spectrum at the output of the two Gaussian filters is shown in Fig. 5. Specifically, Figs. 5(a) and 5(b) depict the spectral and temporal waveforms at the output of branch 1, respectively, while Figs. 5(c) and 5(d) shows the equivalent signals at the output of branch 2. The wavelength-domain signals are measured by substituting the photodetector at the branches' output by an optical spectrum analyzer. It can be appreciated that the temporal waveform presents a shape similar to that of its spectral counterpart, but temporally inverted due to the negative sign of the dispersion parameter. Superposed to the measured waveforms it is plotted the Gaussian fit of their main lobe. As expected, the temporal width of the fitting functions is equal in both channels, and it is found to be $T_d = 479$ ps. Wider temporal pulses lead to the potential use of lower acquisition electronics. This could be obtained either by increasing the dispersion D or by using FBGs with higher bandwidth B_R.
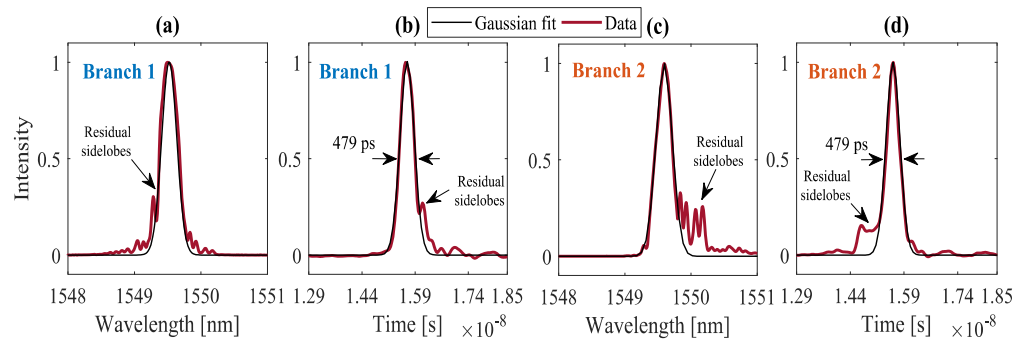

Fig. 5. Normalized waveforms at the output of (a)-(b) branch 1 and (c)-(d) branch 2.

By substituting the measured pulse width into Eq. (4) the FBG bandwidth can be retrieved in order to use the appropriate ACF without the need for a previous grating characterization stage. Moreover, although the residual sidelobes have non-negligible energy contribution (which is especially appreciated at branch 2 in Fig. 5), in the presented method the FBG sidelobes are temporally separated from the main lobe, and thus they do not contribute to the measurement, i.e. the pulse amplitude.

The system performance was tested through the estimation of the central wavelength of the FBG sensor when it was swept from an initial value of 1549.4 nm to a final value of 1549.7 nm. The amplitude comparison function shown in Fig. 4(c) was employed to map the measured pulse amplitude difference into the estimated Bragg wavelength. The measurement results are shown in the scatter plot of Fig. 6, where it is represented the measured Bragg wavelength versus the actual one, together with the residual measurement error. It is seen that the measured error is significantly low and the absolute error does not exceed 20 pm. This wavelength measurement error ultimately determines the uncertainty of the sensed physical parameters in the case of a temperature/strain sensing system. For instance, the grating sensitivity coefficients are measured to be 8 pm/°C and 1.2 pm/µε. Thus, a maximum deviation of 20 pm in the wavelength estimation leads to a maximum error for temperature and strain sensing of 2.5 °C and 16.6 µε, respectively.
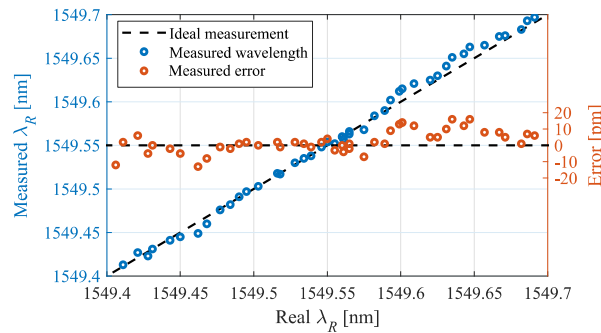
Fig. 6. Wavelength estimation results and residual error.

Table 1 shows a comparison of some characteristics and performance between the different interrogation systems. In the conventional wavelength-to-time mapping measurement systems, the wavelength drift is extracted from temporal shifts and, thus, assuming no timing-jitter, the achievable wavelength resolution $\delta\lambda$ is ultimately determined by the sampling resolution $\delta\tau$ and the dispersion parameter D according to the relation $\delta\lambda = \tau / D$. As an example, a 5 GHz detection bandwidth (10 GSa/s) has $\delta\tau = 100$ ps and a dispersion of $D = 1665$ ps/nm yield to a resolution of $\delta\lambda \approx 60$ pm, which is more than three times the measured error. Moreover, according to the features of the crossed Gaussian filters, the sensitivity in our system can be further improved by increasing the filters' offset.

Table 1. Performance comparison between the different interrogation systems.

Method	Wavelength resolution	Measurement speed	Sidelobes constraint	Cost
Conventional Gaussian-filters	Determined by slope of ACF	Medium-High	Yes	Lower
Wavelength-to-time mapping	Determined by dispersion and sampling rate	High. (dispersion-limited)	No	Medium-High
Proposed method	Determined by slope of ACF	High. (dispersion-limited)	No	Medium-High

The interrogation speed is determined by the laser repetition rate, which should be kept such that there is no temporal overlap between two consecutive pulses even in the pessimistic case in which the FBG experience the maximum but opposite wavelength shifts. In simultaneous to an amplitude variation in the detected waveforms, the Bragg wavelength shift leads to a temporal shift proportional to the system's dispersion. This can be appreciated in Fig. 7, where the detected signals at the output of both branches under different Bragg wavelength shifts ranging from an initial value λ_0 to $\lambda_0 + 294$ pm, are shown. In the experiments, the interrogation period was set to 3.78 ns, yielding an interrogation rate of 264 MHz. The temporal shift experienced by the filtered pulses is τ_{di}, given by Eq. (4). Thus, the repetition period of the probe laser should be higher than the maximum temporal shift difference, $\max(\tau_{di}) - \min(\tau_{di})$, to which it must be added a guard interval that considers pulse width, residual side lobes and detectors relaxation times. Recall that, similarly to the conventional Gaussian-filter technique, the wavelength resolution here is determined by the slope of the ACF and not by the speed of the acquisition electronics. In this case, potential interrogation speeds up to the GHz regime can be reached, while maintaining high resolutions of a few picometers.

Finally, it is worth to note that due to the intrinsic pulsed nature of the source, this method is directly suitable for interrogation of quasi-distributed sensor networks in which several FBGs
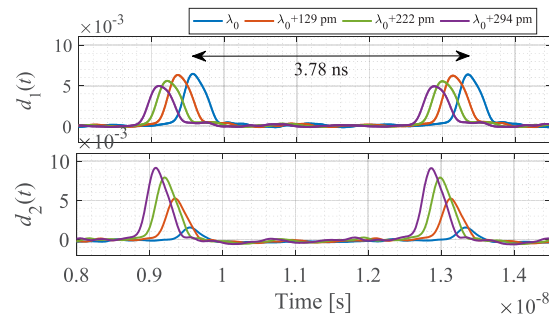
Fig. 7. Acquired signal for different Bragg wavelength shifts. The laser repetition rate is set to 264 MHz.

are multiplexed using TDM and WDM techniques [15,22]. In this case, the source repetition period must be set to be higher than the maximum round-trip time, while the minimum physical separation between sensors in the fiber must be such that to avoid temporal overlap between the reflected pulses corresponding to consecutive FBGs.

4. Conclusions

We have proposed a FBG wavelength monitoring technique based on Gaussian filters and wavelength-to-time mapping of broadband short pulses in a dispersive medium. In the proposed system, the filtered grating spectrum is mapped into a temporal waveform, and the Bragg wavelength is determined from the amplitude difference of the detected pulses at the output of two crossed Gaussian filters. Therefore, the system combines the best features of techniques based on wavelength-to-time mapping and Gaussian intensity filters; an increased linear wavelength range by avoiding measurement distortions arising from residual power from the sensor side lobes, fast interrogation speeds and a high tunable sensitivity that depends on the filters' offset.

We have developed the mathematical background for a general case in which the sensing FBG can have an arbitrary spectral bandwidth. Moreover, we proved that the grating bandwidth can be directly derived from the detected waveforms, which further improves the system in terms of flexibility and real-time operation. Finally, we carried out proof-of-concept experiments and obtained measurement errors of less than 20 pm in simultaneous with ultra-fast acquisition rates of 264 MHz.

Acknowledgments

Disclosures

The authors declare no conflicts of interest

References

1. C. R. Giles, "Lightwave applications of fiber Bragg gratings," J. Lightwave Technol. **15**(8), 1391–1404 (1997).
2. M. P. Fernández, P. A. Costanzo Caso, and L. A. Bulus Rossini, "False Detections in an Optical Coding-Based PON Monitoring Scheme," IEEE Photonics Technol. Lett. **29**(10), 802–805 (2017).

3. D. Sadot and E. Boimovich, "Tunable optical filters for dense WDM networks," IEEE Commun. Mag. **36**(12), 50–55 (1998).

4. M. P. Fernández, L. A. Bulus Rossini, J. P. Pascual, and P. A. Costanzo Caso, "Enhanced fault characterization by using a conventional OTDR and DSP techniques," Opt. Express **26**(21), 27127–27140 (2018).

5. M. P. Fernández, L. A. Bulus Rossini, and P. A. Costanzo Caso, "PON Monitoring Technique Using Single-FBG Encoders and Wavelength-to-Time Mapping," *IEEE Photonics Technol. Lett.*, 2019 (early access) doi: 10.1109/LPT.2019.2944528.

6. M. Burla, L. Romero Cortés, M. Li, X. Wang, L. Chrostowski, and J. Azaña, "Integrated waveguide Bragg gratings for microwave photonics signal processing," Opt. Express **21**(21), 25120–25147 (2013).

7. A. Triana, D. Pastor, and M. Varon, "Code Division Multiplexing Applied to FBG Sensing Networks: FBG Sensors Designed as Discrete Prolate Spheroidal Sequences (DPSS-FBG Sensors)," J. Lightwave Technol. **35**(14), 2880–2886 (2017).

8. D. Monzón-Hernández, J. Mora, P. Pérez-Millán, A. Díez, J. L. Cruz, and M. V. Andrés, "Temperature sensor based on the power reflected by a Bragg grating in a tapered fiber," Appl. Opt. **43**(12), 2393–2396 (2004).

9. A. D. Kersey, M. A. Davis, H. J. Patrick, M. LeBlanc, K. P. Koo, C. G. Askins, M. A. Putnam, and E. J. Friebele, "Fiber grating sensors," J. Lightwave Technol. **15**(8), 1442–1463 (1997).

10. Y. Sano and T. Yoshino, "Fast optical wavelength interrogator employing arrayed waveguide grating for distributed fiber Bragg grating sensors," J. Lightwave Technol. **21**(1), 132–139 (2003).

11. M. A. Davis and A. D. Kersey, "All-fibre Bragg grating strain-sensor demodulation technique using a wavelength division coupler," Electron. Lett. **30**(1), 75–77 (1994).

12. H. Xia, C. Wang, S. Blais, and J. Yao, "Ultrafast and precise interrogation of fiber Bragg grating sensor based on wavelength-to-time mapping incorporating higher order dispersion," J. Lightwave Technol. **28**(3), 254–261 (2010).

13. C. Wang and J. Yao, "Ultrafast and ultrahigh-resolution interrogation of a fiber Bragg grating sensor based on interferometric temporal spectroscopy," J. Lightwave Technol. **29**(19), 2927–2933 (2011).

14. M. Lei, W. Zou, X. Li, and J. Chen, "Ultrafast FBG Interrogator Based on Time-Stretch Method," IEEE Photonics Technol. Lett. **28**(7), 778–781 (2016).

15. L. Ma, C. Ma, Y. Wang, D. Y. Wang, and A. Wang, "High-Speed Distributed Sensing Based on Ultra Weak FBGs and Chromatic Dispersion," IEEE Photonics Technol. Lett. **28**(12), 1344–1347 (2016).

16. R. Cheng, L. Xia, J. Zhou, and D. Liu, "Wavelength interrogation of fiber Bragg grating sensors based on crossed optical Gaussian filters," Opt. Lett. **40**(8), 1760–1763 (2015).

17. R. Cheng, L. Xia, Y. Ran, J. Rohollahnejad, J. Zhou, and Y. Wen, "Interrogation of Ultrashort Bragg Grating Sensors Using Shifted Optical Gaussian Filters," IEEE Photonics Technol. Lett. **27**(17), 1833–1836 (2015).

18. R. Cheng, L. Xia, C. Sima, Y. Ran, J. Rohollahnejad, J. Zhou, Y. Wen, and C. Yu, "Ultra-short FBG based distributed sensing using shifted optical Gaussian filters and microwave-network analysis," Opt. Express **24**(3), 2466–2484 (2016).

19. K. Goda and B. Jalali, "Dispersive Fourier transformation for fast continuous single-shot measurements," Nat. Photonics **7**(2), 102–112 (2013).

20. M. P. Fernández, L. A. Bulus Rossini, and P. A. Costanzo Caso, "Method for real-time measurement of the nonlinear refractive index," AIP J, Appl. Phys. **126**(9), 093104 (2019).

21. T. Erdogan, "Fiber grating spectra," J. Lightwave Technol. **15**(8), 1277–1294 (1997).

22. L. Xia, Y. Wu, U. Rahubadde, and W. Li, "TDM Interrogation of Identical Weak FBGs Network Based on Delayed Laser Pulses Differential Detection," IEEE Photonics J. **10**(3), 1–8 (2018).